

Selective Visual Detection of TNT at the Sub-Zeptomole Level**

Ammu Mathew, P. R. Sajanlal, and Thalappil Pradeep*

Dedicated to Professor P. T. Manoharan on the occasion of his 77th birthday

Realizing the limits of sensitivity, while maintaining selectivity, is an ongoing quest. Among the multitude of requirements, national security, early detection of diseases, safety of public utilities, and radiation prevention are some of the areas in need of ultralow detection.^[1] Structural, functional, and electronic features of nanomaterials are used to develop reliable analytical methods.^[2] Several kinds of surface-enhanced spectroscopy, surface-enhanced Raman in particular, can be used for such applications;^[3] the technique may be further enhanced by spatially separating the analyte and the active plasmonic nanostructure with an insulator, a method known as shell-isolated nanoparticle-enhanced Raman spectroscopy (SHINERS).^[4] Creating uniform anisotropic structures with nanoscale attributes by simple solution chemistry and combining analyte-selective chemistry on such surfaces enables ultrasensitive and selective detection methods.^[5] Noble metal quantum clusters (QCs),^[6] a new family of atomically precise nanomolecules with intense luminescence, along with their protein protected analogues,^[6c] are highly sensitive and selective for specific analytes.^[7] Anchoring such QCs on mesoscale (100 nm to a few μm) particles leads to surface-enhancement of their luminescence^[7c] and can create a new platform for ultrasensitive detection, especially when combined with the use of optical microscopy. Gold mesoflowers (MFs) are anisotropic materials with unique five-fold symmetric stems^[8] containing surface-enhancing nanoscale features. An entire MF is only a few micrometers in size, and its distinct shape allows for unique identification by optical microscopy; thus, changes in the properties of an MF can be used for the immediate and efficient detection of analytes. Herein, we demonstrate the selective detection of 2,4,6-trinitrotoluene (TNT) at the sub-zeptomole level (10^{-21} moles) through a combination of these strategies on a mesostructure.

Our method involves anchoring silver clusters,^[9] which are comprised of fifteen atoms and embedded in bovine serum albumin (BSA), on silica-coated Au MFs, termed

$\text{Au@SiO}_2\text{@Ag}_{15}$ MFs, and using this system for analyte detection. Syntheses of the various components are described in the experimental section. The Au@SiO_2 MFs have a tip-to-tip length of ca. 4 μm (Supporting Information, Figure S1 a). The BSA-protected silver cluster (Ag_{15}), is a red luminescent water-soluble QC prepared by a previously reported procedure (see Figure S2 for essential characterization data).^[9] Apart from a high quantum yield (10.7%) in water, it is stable over a wide pH range and exhibits emission in the solid state. We exposed varying concentrations of TNT to $\text{Au@SiO}_2\text{@Ag}_{15}$ MFs and found that even a concentration of less than one zeptomole of TNT per mesoflower quenches the luminescence of the composite mesoflowers within 1 min. The simultaneous disappearance of the luminescence of Ag_{15} on the MF and the appearance of the luminescence of another embedded fluorophore allows for easy identification of the analyte. Characterization data for the various composite MFs used in this study are presented in the Supporting Information.

The hybrid structures, $\text{Au@SiO}_2\text{@Ag}_{15}$ MFs, with unique structural attributes are observable under an optical microscope (see Figure S3 for a schematic of the setup used). Dark field microscopic images of these MFs show their well-defined features; they are star-shaped in a two dimensional projection (Figure 1 A). The fluorescence image of the same MF (ca. 490 nm excitation, emitted light was passed through a triple-pass filter and imaged) shows a characteristic red emission owing to the QCs anchored on its surface (Figure 1 A). Unlike with other spherical single particle sensors, which are difficult to locate and distinguish by light-based microscopy, the well-defined shapes of the MFs ensure that the desired particles alone are analyzed. Furthermore, the analyte adsorption capacity of the MFs is enhanced by the thin inert layer of silica employed as a base. Au core/silica shell structures of this type can provide enhanced fluorescence and Raman scattering. The better stability of the QCs on the silica layer, along with a reduction in the luminescence quenching of the QCs on the MF surface and ease of functionalization are among the added advantages of this material (see the Supporting Information).

Exposure of the $\text{Au@SiO}_2\text{@Ag}_{15}$ MFs to TNT (2.5 μL) at a concentration of one part per trillion (ppt) decreases the luminescence intensity slightly without affecting the optical image (Figure 1 B), whereas at one part per billion (ppb) of TNT the luminescence feature disappears completely (Figure 1 C; note that the MFs shown in Figure 1 A–C are different in each case). For spectral intensity data collected from the surface of these MFs, see the Supporting Information, Figure S4. The quenching of cluster luminescence is due to the formation of a Meisenheimer complex^[5c,11] by the

[*] A. Mathew, Dr. P. R. Sajanlal,^[†] Prof. T. Pradeep
DST Unit of Nanoscience (DST UNS), Department of Chemistry,
Indian Institute of Technology Madras
Chennai 600036 (India)
E-mail: pradeep@iitm.ac.in

[†] Current address: Laser Dynamics Laboratory, School of Chemistry
and Biochemistry, Georgia Institute of Technology
Atlanta, GA 30332-0400 (USA)

[**] We thank the Department of Science and Technology, Government
of India for constantly supporting our research program on
nanomaterials. A.M. thanks CSIR for a research fellowship.

Supporting information for this article is available on the WWW
under <http://dx.doi.org/10.1002/anie.201203810>.

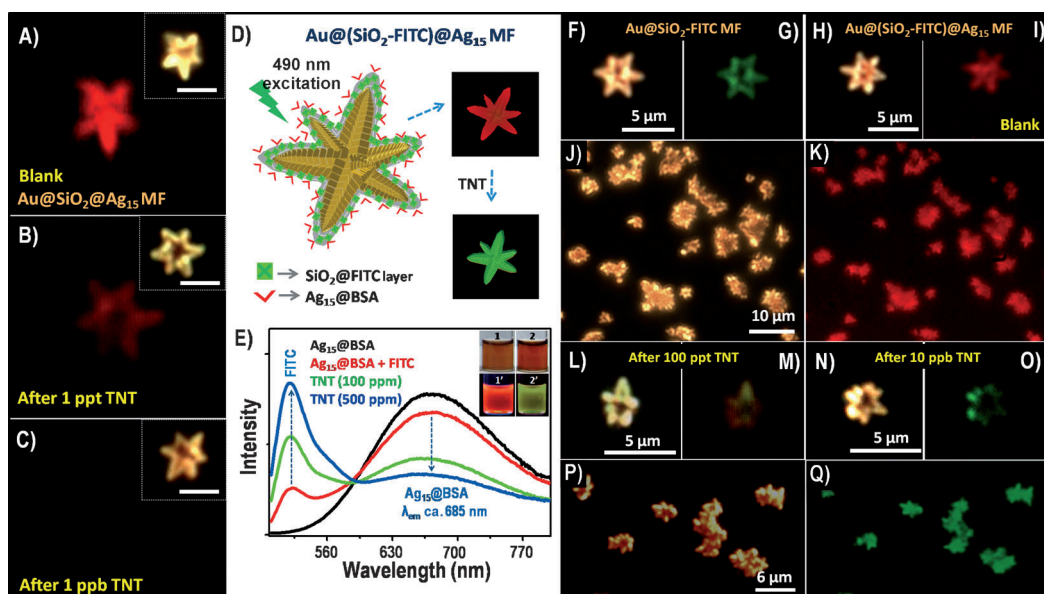


Figure 1. A–C) Fluorescence images (ca. 490 nm excitation) of Au@SiO₂@Ag₁₅ MFs taken using a dark field fluorescence microscope. Insets show the optical images corresponding to the fluorescence images; scale bars are 3 μm. Conditions under which the images are taken are specified on the figures, see the Experimental Section for details. D) Illustration of the sensor and the TNT detection approach; insets depict the sensing particle before (red) and after exposure to TNT (green). E) Effect on the emission spectra of the bare cluster upon mixing with FITC dye and subsequent exposure to TNT solutions of varying concentrations; inset shows photographs of a solution containing a mixture of FITC dye and Ag₁₅ clusters before and after TNT addition, taken under visible (1 and 2) and UV light (1' and 2'), respectively. The cluster emission (red) and FITC emission (green) are clearly observable. F–I and L–O) Optical and fluorescence images of Au@(SiO₂-FITC) MFs before (F,G) and after (H,I) cluster functionalization, as well as after exposure to TNT at concentrations of 100 ppt (L,M) and 10 ppb (N,O). J,K,P,Q) Large-area optical (J,P) and fluorescence (K,Q) images before (J,K) and after (P,Q) 10 ppb TNT exposure, respectively.

chemical interaction between TNT and the free amino groups in BSA. The solution turned dark red and the formation of the complex was confirmed by the emergence of features at 340, 450, and 525 nm in the UV absorption spectra (Figure S5). The specificity of the Meisenheimer complexation makes the cluster selective for TNT; closely related molecules, such as 2,4-dinitrotoluene (2,4-DNT), cyclotrimethylenetrinitramine (RDX), and 4-nitrotoluene do not quench its luminescence at this concentration (Figures S4 and S5). Note that no change in absorption features was observable when the concentration of TNT was < 10 ppm in bulk solution phase measurements (Figure S5), thus indicating the limit of TNT detection by Ag₁₅ clusters in solution. However, at the single particle level a spectral change occurred even at 1 ppt, as shown in the inset in Figure S4A. Luminescence spectra at identical concentrations (100 parts per million (ppm)) both in the solution phase and at the single particle level are compared in Figure S4B. Although the presence of tryptophan in BSA gives it an intrinsic blue fluorescence with excitation and emission maxima at 295 and 332 nm, respectively, it showed only a slight quenching in presence of TNT (Figure S4C). This poor response of the tryptophan fluorescence to the interaction of the protein with TNT may be due to the distance between the former and the free amine groups in the same protein subdomain. In the case of Ag₁₅, drastic quenching in the cluster luminescence was observed. This may either be attributed to the anionic σ complex formed and the subsequent sensitivity of the cluster to its immediate environment,

or as a result of the fluorescence resonance energy transfer between the cluster core and the protein.

For ease of visual detection, a change in the luminescence color in the presence of an analyte is a more desirable indicator than the disappearance/quenching of luminescence. Therefore, a TNT-insensitive fluorophore with the same excitation energy, but with a different emission wavelength, was pre-coated on the Au@SiO₂ MFs prior to cluster functionalization. An illustration of the procedure and the detection approach is shown in Figure 1D. We used fluorescein isothiocyanate (FITC) as the dye, which resulted in a bright green emission from the Au@SiO₂-FITC MFs (Figure 1G). The fluorescence spectrum collected from such a single particle is shown in Figure S4D. The emission observed around 540 nm clearly indicates the adsorption of FITC onto the Au@SiO₂ MFs. After further functionalization with Ag QCs, the Au@(SiO₂-FITC)@Ag₁₅ MFs showed a red emission (Figure 1I) wherein the FITC emission is suppressed. Upon exposure to 10 ppb TNT, a green emission from the underlying FITC was observed (Figure 1O), as the red luminescence from the cluster had been completely quenched. Even at 100 ppt, an observable color change was evident (Figure 1M). Large area images of the MFs before (Figure 1J and K) and after TNT exposure (Figure 1P and Q) confirm that the change occurs uniformly on all MFs. This uniformity is important in the development of a reliable method. The observation of green luminescence is in agreement with the solution phase data, wherein the disappearance

of cluster emission and the emergence of FITC emission are observed upon TNT exposure (Figure 1E).

Combining several analytical methods at the single particle level makes the detection more foolproof. Owing to their highly anisotropic nature, MFs can act as highly sensitive probes for surface-enhanced Raman spectroscopy (SERS). Bimetallic Ag-coated Au MFs (Au/Ag MFs)^[12] are yet another type of MF (see the Experimental Section for synthetic details), which allow for ultrasensitive Raman detection, as compared to bare MFs. When coated directly on Au/Ag MFs, Ag QCs result in unique metal-enhanced luminescence^[13] (Figures S3a and S6). Upon exposure to TNT, luminescence from the QCs on the MFs are lost and the Raman features from TNT (at 1209, 1361, 1535, 1619 and 2960 cm^{-1}) are detectable on the particle at 633 nm excitation. The gradual evolution of the Raman features of TNT as the concentration of TNT increases is shown in Figure 2A. The appearance of specific TNT features (Figure S7) ensures that

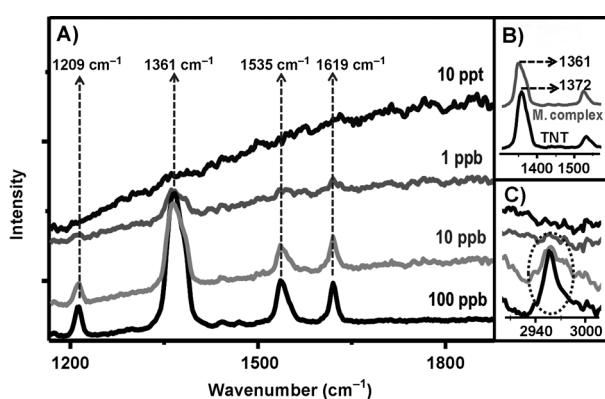


Figure 2. A) Raman spectra showing the gradual evolution of TNT features as the concentration of TNT added to Au/Ag@Ag₁₅ MFs increases. B) Comparison of the symmetric and asymmetric NO₂ stretching bands in the SERS spectra of TNT before (black) and after Meisenheimer complex formation (gray). C) The gradual appearance of a Raman band at 2960 cm^{-1} .

the observed changes are exclusively due to this analyte. Such changes were not observable with other analytes (Figure S7). The Meisenheimer complex formation was confirmed by comparing the SERS spectra of TNT before and after complexation (Figure 2B). After complex formation, the symmetric and asymmetric stretching bands of the NO₂ group, observed in TNT at 1372 and 1545 cm^{-1} , respectively, were shifted to 1361 and 1535 cm^{-1} , respectively. This marked decrease in the vibrational frequencies can be attributed to electron delocalization in the ring and a post-complexation reduction in symmetry. The emergence of a peak at 2960 cm^{-1} (Figure 2C) may also be attributed to the Meisenheimer complex formed (NH₂ symmetric stretch),^[5c] but the same region also corresponds to the C–H stretching and CH₂ asymmetric stretching vibrations of TNT, which makes an exact assignment difficult. By combining the high sensitivity and selectivity offered by SERS with our sensing method, we enhance the accuracy and reliability of the detection technique.

As both the measurements are conducted at the single particle level, the number of molecules actually responsible for the observed changes is very small. Taking the dimension of a single MF as 4 μm , the volume of the analyte solution required to completely wet the MF surface can be taken as 34 femtoliters. For a 100 ppt TNT solution, this volume amounts to 0.015 zeptomoles, or ca. nine molecules of TNT. Thus, detection at far below the zeptomole level is demonstrated with this strategy. As two methods of analysis are combined at the single particle level, it is unlikely that false positives are possible. The principal advantage of this method is that only a single particle is required for the detection of an analyte, allowing for the miniaturization of devices. The amount of gold required to make one MF with a 4 μm edge length is ca. 0.288 ng, and it can be recovered and reused. Although the molecular details of the detection chemistry are complex, the procedure itself is simple.

A similar strategy can be employed for metal ion sensing. QCs are known for the selective sensing of Hg²⁺ ions in solution.^[14] The interaction of mercury with the metal core of the QCs has been proposed as a possible reason for this effect. In this case, Hg²⁺ ions were selectively visually detected at the zeptomole level among other metal ions such as Pb²⁺, Ni²⁺, Cd²⁺, and Cu²⁺ (Figure S8). Even though the luminescence of the Ag₁₅ cluster was quenched for both Cu²⁺ and Hg²⁺ ions upon treatment of a 100 ppm solution of metal ions with the cluster solution (Figure S8A), at the single particle level, a ca. 99% quenching of cluster luminescence was observed only for Hg²⁺ ions (Figure S8C–H). Spectral intensity data collected from the surface of the MFs in each case are shown in Figure S8I. Ag₁₅ clusters showed selective luminescence quenching in the presence of Hg²⁺ ions when treated with a mixture of metal ions (Figure S8B). A bar diagram illustrating the relative variation in the luminescence intensity in the solution phase and at the single particle level at 100 ppm of metal ions is shown in Figure 3G. Here, the relative intensities are comparable, except for Cu²⁺ and Hg²⁺, where the quenching of cluster luminescence at the single particle level was much more pronounced, especially for the latter. At still lower concentrations (<10 ppm) we did not observe any quenching for Cu²⁺ ions, whereas luminescence from the MF was completely quenched for Hg²⁺, even at 1 ppb (Figure 3C). Data collected from the surface of the MFs showed a decrease in spectral intensity from that collected from blank Au@SiO₂@Ag₁₅ MFs, up to a 10 ppt concentration of Hg²⁺ (Figure S8J). The gradual disappearance of the luminescence intensity from the MF surface upon exposure to Hg²⁺ of varying concentrations (10 ppt–1 ppb) is depicted in Figure 3A–C. Though a distinct color change (red to yellow) was observable even at a Hg²⁺ concentration of 500 ppt (Figure 3E), the MF appeared green at 1 ppb (Figure 3F). The yellow color observed may be due to the additive effect of the unquenched red luminescence of the cluster on the MF surface and the underlying green luminescence of FITC-incorporated silica shell. This easily observable color change (red to green) in the presence of Hg²⁺ in solution enables the visual detection of such ions at the ppt level by our hybrid single particle sensor. When 2.5 μL of a 500 ppt Hg²⁺ solution (ca. 2 picograms) is used to wet the

- Rev. **2008**, *37*, 955; e) X. Huang, I. H. El-Sayed, W. Qian, M. A. El-Sayed, *Nano Lett.* **2007**, *7*, 1591.
- [4] J. F. Li, Y. F. Huang, Y. Ding, Z. L. Yang, S. B. Li, X. S. Zhou, F. R. Fan, W. Zhang, Z. Y. Zhou, Y. WuDe, B. Ren, Z. L. Wang, Z. Q. Tian, *Nature* **2010**, *464*, 392.
- [5] a) M. Li, Q. Wang, X. Shi, L. A. Hornak, N. Wu, *Anal. Chem.* **2011**, *83*, 7061; b) K. Zhang, H. Zhou, Q. Mei, S. Wang, G. Guan, R. Liu, J. Zhang, Z. Zhang, *J. Am. Chem. Soc.* **2011**, *133*, 8424; c) S. S. R. Dasary, A. K. Singh, D. Senapati, H. Yu, P. C. Ray, *J. Am. Chem. Soc.* **2009**, *131*, 13806.
- [6] a) S. Choi, R. M. Dickson, J. Yu, *Chem. Soc. Rev.* **2012**, *41*, 1867; b) M. A. H. Muhammed, T. Pradeep in *Advanced Fluorescence Reporters in Chemistry and Biology II, Vol. 9* (Ed.: A. P. Demchenko), Springer, Berlin, **2010**, part 4, pp. 333–353, and references therein; c) P. L. Xavier, K. Chaudhari, A. Baksi, T. Pradeep, *Nano Rev.* **2012**, *3*, 14767; d) T. U. B. Rao, B. Nataraju, T. Pradeep, *J. Am. Chem. Soc.* **2010**, *132*, 16304; e) T. Udayabhaskararao, Y. Sun, N. Goswami, S. K. Pal, K. Balasubramanian, T. Pradeep, *Angew. Chem.* **2012**, *124*, 2197; *Angew. Chem. Int. Ed.* **2012**, *51*, 2155; f) I. Díez, M. Pusa, S. Kulmala, H. Jiang, A. Walther, A. S. Goldmann, A. H. E. Müller, O. Ikkala, R. H. A. Ras, *Angew. Chem.* **2009**, *121*, 2156; *Angew. Chem. Int. Ed.* **2009**, *48*, 2122.
- [7] a) M. A. Habeeb Muhammed, T. Pradeep, *Chem. Phys. Lett.* **2007**, *449*, 186; b) Y. H. Lin, W. L. Tseng, *Anal. Chem.* **2010**, *82*, 9194; c) W. Y. Chen, G. Y. Lan, H. T. Chang, *Anal. Chem.* **2011**, *83*, 9450; d) X. Yuan, T. J. Yeow, Q. Zhang, J. Y. Lee, J. Xie, *Nanoscale* **2012**, *4*, 1968; e) M. A. Habeeb Muhammed, P. K. Verma, S. K. Pal, A. Retnakumari, M. Koyakutty, S. Nair, T. Pradeep, *Chem. Eur. J.* **2010**, *16*, 10103.
- [8] P. R. Sajanlal, T. Pradeep, *Nano Res.* **2009**, *2*, 306.
- [9] A. Mathew, P. R. Sajanlal, T. Pradeep, *J. Mater. Chem.* **2011**, *21*, 11205.
- [10] a) O. G. Tovmachenko, C. Graf, D. J. van den Heuvel, A. van Blaaderen, H. C. Gerritsen, *Adv. Mater.* **2006**, *18*, 91; b) A. R. Guerrero, R. F. Aroca, *Angew. Chem.* **2011**, *123*, 691; *Angew. Chem. Int. Ed.* **2011**, *50*, 665.
- [11] a) L. Yang, L. Ma, G. Chen, J. Liu, Z.-Q. Tian, *Chem. Eur. J.* **2010**, *16*, 12683; b) D. Gao, Z. Wang, B. Liu, L. Ni, M. Wu, Z. Zhang, *Anal. Chem.* **2008**, *80*, 8545; c) Y. Engel, R. Elnathan, A. Pevzner, G. Davidi, E. Flaxer, F. Patolsky, *Angew. Chem.* **2010**, *122*, 6982; *Angew. Chem. Int. Ed.* **2010**, *49*, 6830; d) Y. Xia, L. Song, C. Zhu, *Anal. Chem.* **2011**, *83*, 1401.
- [12] P. R. Sajanlal, T. Pradeep, *Langmuir* **2010**, *26*, 8901.
- [13] K. Aslan, J. R. Lakowicz, C. D. Geddes, *J. Phys. Chem. B* **2005**, *109*, 6247.
- [14] a) J. Xie, Y. Zheng, J. Y. Ying, *Chem. Commun.* **2010**, *46*, 961; b) C. C. Huang, Z. Yang, K. H. Lee, H. T. Chang, *Angew. Chem.* **2007**, *119*, 6948; *Angew. Chem. Int. Ed.* **2007**, *46*, 6824.

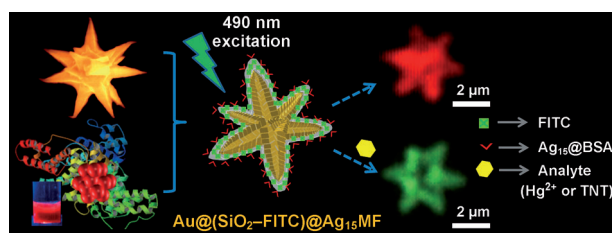


Sensors

A. Mathew, P. R. Sajanlal,

T. Pradeep*     

Selective Visual Detection of TNT at the Sub-Zeptomole Level



How low can you go? The visual detection of 2,4,6-trinitrotoluene and Hg^{2+} at the sub-zeptomole level is demonstrated. This was achieved using a hybrid material

that allowed for the development of a single-particle, single-molecule detection technique, which may be the ultimate in ultra-trace sensitivity with selectivity.